Available online at www.sciencedirect.com
SCIENCE DIRECT®
Planetary and Space Science 54 (2006) 200–211
Planetary and Space Science
www.elsevier.com/locate/pss

A pre-shock event at Jupiter on 30 January 2001

Karoly Szego[a,*], David T. Young[b], Thorsten Bagdonat[c], Bruce Barraclough[d], Jean-Jacques Berthelier[e], Andrew J. Coates[f], Frank J. Crary[b], Michele K. Dougherty[g], Geza Erdos[a], Donald A. Gurnett[h], William S. Kurth[h], Andrea Opitz[a], Abi Rymer[f], Michelle F. Thomsen[d]

[a]*KFKI Research Institute for Particle and Nuclear Physics, Budapest, Hungary*
[b]*Southwest Research Institute, San Antonio, TX, USA*
[c]*TU Braunschweig, Germany*
[d]*Los Alamos National Laboratory, Space and Atmospheric Science Group, USA*
[e]*Centre d'Étude des Environnements Terrestre et Planetaires, IPSL, France*
[f]*University College London, Mullard Space Science Laboratory, UK*
[g]*Imperial College, London, UK*
[h]*Department of Physics and Astronomy, The University of Iowa, Iowa City, Iowa, USA*

Received 7 August 2004; received in revised form 22 October 2005; accepted 27 October 2005
Available online 27 December 2005

Abstract

In this paper we analyze a pre-shock event that we observed in the foot region of the quasi-parallel bow shock (BS) that the Cassini spacecraft crossed on 30 January 2001, at about 1030 UT. Before crossing the BS, the incoming solar wind first decelerated, and then the bulk velocity both of the proton and α components increased, the flow accelerated and decelerated, heated and cooled several times. We characterize the plasma in the foot using the data measured by the magnetometer, the radio and plasma wave science (RPWS) instrument, and the Cassini plasma spectrometer (CAPS) being carried onboard the Cassini spacecraft, and analyze the observations. We argue that the velocity and temperature changes can be caused by firehose instabilities excited by ions reflected from the shock. We investigate another possibility, shocklet formation, to account for the observed features, but conclude that this explanation seems to be less likely. In the foot we also identified both backstreaming electrons and ions and electrostatic waves in the 100–1000 Hz range very likely excited by the backstreaming electrons.

Keywords: Foot region; Bow shock; Firehose instability; Planetary magnetospheres

1. Introduction

The Cassini spacecraft on its way to Saturn explored the plasma environment of Jupiter near the ecliptic plane, on the dusk side of the planet. The spacecraft trajectory is shown in Fig. 1 in the Jupiter Solar Equatorial (JSEQ) frame of reference (see figure caption for the definitions of the coordinate system).

The first bow shock (BS) crossing took place on 30 December 2000, and it was followed by more than forty crossings. The structure of the BS transition layer was frequently not conventional as we approached the flanks; some of these crossings are discussed by Szego et al. (2003) pointing out their conspicuous features: the shock was turbulent and very dynamic, magnetic fluctuations were superimposed on the shock. In several cases the field data were too smeared to pinpoint the shock transition, but the onset of ion thermalization was always a good indicator of the shock location. In the literature there seems to be an agreement that the Jovian BS might be very different from the shocks observed around the terrestrial planets (Joy et al., 2002; Huddleston et al. 1998, and references cited therein). The huge size (several tens of million kilometers from the nose to the flanks) has the consequence that it takes days till the solar wind reaches the flank, and the

*Corresponding author. Tel.: +36 1 411 6367; fax: +36 1 411 6244.
E-mail address: szego@rmki.kfki.hu (K. Szego).

0032-0633/$ - see front matter © 2005 Elsevier Ltd. All rights reserved.
doi:10.1016/j.pss.2005.10.011

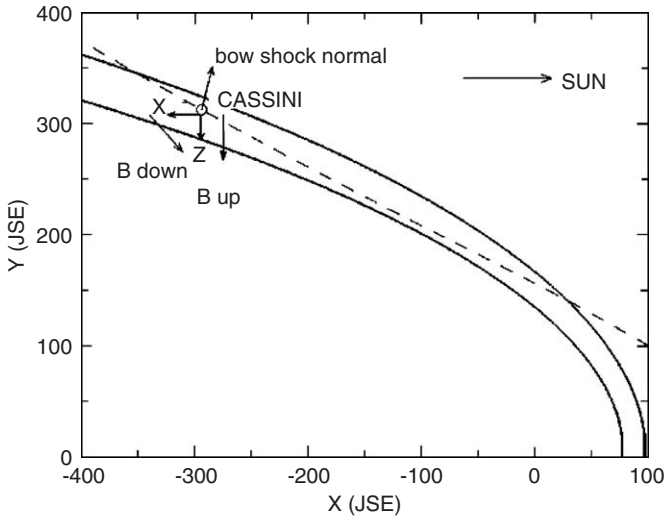

Fig. 1. Cassini's orbit is shown in the Jupiter Solar Equatorial frame of reference. (In JSEQ the z-axis is along Jupiter's spin axis, and the x–z-plane contains the Sun). The plot shows the location of Cassini at 10:30 UT on 30 January 2001. In addition, the plot shows the Joy et al. (2002) shock models at the 50% and 75% confidence intervals for being in the solar wind. The shock normal (0.244, 0.963, −0.118) that is shown was derived by minimum variance analysis of 24 s samples over the interval between 07:30 and 14:50 UT and is in good agreement with the Joy et al. shock model. The upstream (0.02, −1.00, 0.00) nT and downstream (0.73, −0.83, 1.65) nT field directions are 4 h averages of the 24 s field data (starting at 06:10 and 20:24 UT, respectively). The x–y-axes of the spacecraft reference system (SCRS) are also exhibited in the JSEQ x–y-plane. (The authors are indebted to a colleague who prepared this figure but wanted to remain anonymous.)

few-hour variability of the solar wind at 5.2 AU may prevent the shock front from reaching stability during this period of time. The high Mach number of the solar wind due to its low density may result in new features because the second critical Mach number can be exceeded around the nose of the BS which means that the conventional dissipation processes may no longer be adequate to stabilize the shock front (Quest, 1985). An additional complication is that the obstacle itself—due to the rapid rotation of Jupiter and the large size of the system—is a quickly changing magnetodisk (Engel and Beard, 1980). Therefore, it is conceivable that the Jovian BS may seldom stay in a steady state, if it is reached at all.

The BS crossing we investigate here was a quasiparallel shock, as we shall show below. The MHD theory of quasi-parallel shocks is summarized in Kennel et al. (1985) and the references cited therein. The first studies focused on how wave steepening can lead to the shock formation. In those studies it was pointed out that because the shock compression would only increase the temperature parallel to the magnetic field, the firehose instability could grow downstream. These studies assumed high β plasma (β is the ratio of the thermal to magnetic pressure, $\beta = 0.4n(\mathrm{cm}^{-3})T(\mathrm{eV})B^{-2}(\mathrm{nT})$), and did not consider upstream and foot phenomena. The upstream region was modeled later by the injection of ion beams into the foreshock leaked or reflected back from the downstream region. A numerical simulation of such shock transitions was carried out by Quest (1988) based on the fact that the downstream particles can easily escape upstream along the parallel field lines; more details of this model will be given below. This model allows the firehose instability to develop in the foot, a possibility that is the focal point of the current study. We note here that the plasma β at Jupiter can be two orders of magnitude lower than at Earth due to the decrease of all parameters characterizing β. This is also an important difference between these two planets. The typical plasma β of the solar wind near Jupiter was of the order of 0.1 during the Cassini flyby.

Pre-shock events, that are events occurring on the upstream side of the shock due to kinetic effects associated with shock formation, are well known at planets and other solar system bodies. The observed phenomena show broad variety depending on the solar wind conditions, obstacle properties, shock structure, and the location of the observation. The Voyager 1 spacecraft made the first wave measurements at Jupiter (Scarf et al., 1979); these have led to many important discoveries. We cite here only those that have relevance to the current study. It was found by Moses et al. (1990) that in properly normalized units the wave amplitudes of electrostatic waves at the outer planets can be several orders of magnitude higher than at Earth, and thus more likely to be significant participants in the shock processes. A new electrostatic wave mode with center frequency below the electron plasma frequency and above the maximum frequency for Doppler-shifted ion acoustic waves was found by Moses et al. (1984). The same authors pointed out that the excitation mechanism was consistent with modes generated by strong electron heat flux. Further properties of the Jovian foot were summarized by Scarf et al. (1987). However, a systematic study of the Jovian foot region is not available in the literature.

The foot region exhibited surprising plasma behavior on 30 January 2001, before 10:30 UT, as observed by the plasma instruments carried onboard the Cassini spacecraft. In the foot region of the BS the solar wind plasma exhibited large excursions both in bulk velocity and temperature. Another feature of this event was that the combination of field geometry, flow direction, and shock orientation allowed the foreshock region to extend well in front of the shock. Moreover, the shallow crossing angle of the spacecraft with respect to the foot allowed its features to be sampled over hours rather than minutes. This confluence of geometric conditions makes this event interesting to study. In this paper we summarize these observations and provide a possible explanation concerning this event.

2. Instrumentation and the geometry of the event

Cassini carries onboard a full set of plasma measuring instruments. The results presented here are based on the data collected by the magnetometer (MAG) (Dougherty

et al., 2004), the radio and plasma wave science (RPWS) instrument (Gurnett et al., 2004) and the Cassini plasma spectrometer (CAPS) (Young et al., 2004). The MAG has several modes of operation; we use here 24-s resolution data products. RPWS acquires amplitudes of wave electric fields from approximately 1 Hz to 16 MHz and wave magnetic fields from approximately 1 Hz to 12 kHz, providing a spectrum once per 32–64 s, depending on the instrument mode. In this paper we use the electric field data only. The sensor geometry is described in Gurnett et al. (2004).

The CAPS instrument has three independently operated sensors: the ion mass spectrometer (IMS) designed to analyze ion composition and plasma dynamics, the electron spectrometer (ELS), and the ion beam spectrometer (IBS) to measure narrow, beam-like distributions without mass separation. In the 2 kbps telemetry mode used in this paper CAPS–ELS (Linder et al., 1998) measured electron spectra in 64 logarithmic energy steps between 1 eV and 30 keV. The 160° elevation field of view is split into 20°-wide angular channels, and one such spectrum was collected every 32 s. The ion beam spectrometer, CAPS–IBS, has three entrance apertures offset by 30°, and each field of view is $1.5^\circ \times 150^\circ$. CAPS–IBS collected all ions in 256 specially selected narrow energy steps between ~200 eV and ~9.5 keV with energy resolution $\Delta E/E = 0.015$; one energy sweep was taken in 2 s. In the 2 kbps telemetry mode, 16 sweeps were added during a 32-s-long time interval. The field of view in the azimuth direction was 5° for ELS, and 1.5° for IBS. The whole CAPS package was actuated around a rotation axis parallel to the z-axis of the spacecraft; the highest actuation speed is ~1°/s. The viewing geometry of the three CAPS–IBS fans is shown in Fig. 2. Due to a specific instrument problem, the IMS ion data are not usable for this time interval.

On 30 January 2001 at 0000 UT, Cassini was at a distance of 424.5 R_J ($1R_J = 71,492$ km) from Jupiter, ~47° behind the terminator line in JSEQ, and ~0.5° below the equatorial plane, on the dusk side of the planet (c.f. Fig. 1). The "nominal" shock normal direction in the ecliptic plane at this location, as derived by Joy et al. (2002) based on the statistical analysis of the locations of the BS measured by previous missions, is exhibited in Fig. 1. The spacecraft was three-axis stabilized; starting at 0830 UT and ending at 0850 UT, the spacecraft was rotated until its $-x$-axis pointed towards the Sun; thereafter, the solar wind was sampled more frequently. The spacecraft z-axis pointed generally towards the planet, and the inclination of the spacecraft z-axis to the Jovian equatorial plane (that is in JSEQ, see the caption of Fig. 1 for its definition) was about 9° to the North. The stability of the spacecraft axes during the period we investigate was better than 1°. In this paper, when we refer to the spacecraft reference system (SCRS), we mean its attitude after 0850 UT, because we focus on plasma events between 0850 and 1030 UT.

After the attitude change the spacecraft velocity vector was (−9.3, 5.25, −0.73) km/s in JSEQ, and Cassini flew towards the shock crossing point with a speed of 10.7 km/s. Assuming a stationary shock front, the spacecraft approached it with ~2.9 km/s along the shock normal direction shown in Fig. 1. Before the attitude change the direction of the z-axis of the spacecraft in JSEQ was (−.73, −.68, .02)—that is, it inclined to the ecliptic by ~43°—and CAPS' actuator rotated about the spacecraft z-axis between −79° and 102° relative to the spacecraft $-y$-axis; the solar wind was in the field of view of IBS. The 32-s-long data acquisition time interval was not in phase with the motion of the actuator, therefore the common parts of those actuator intervals in which the solar wind was seen, gave a crude estimate of the solar wind direction, assuming its stability. This direction was within 10° relative to the solar direction. After 0850 UT the range of actuation was decreased (49°–102°), the solar wind (coming supposedly from ~90° actuator angle) was more frequently in the field of view of IBS.

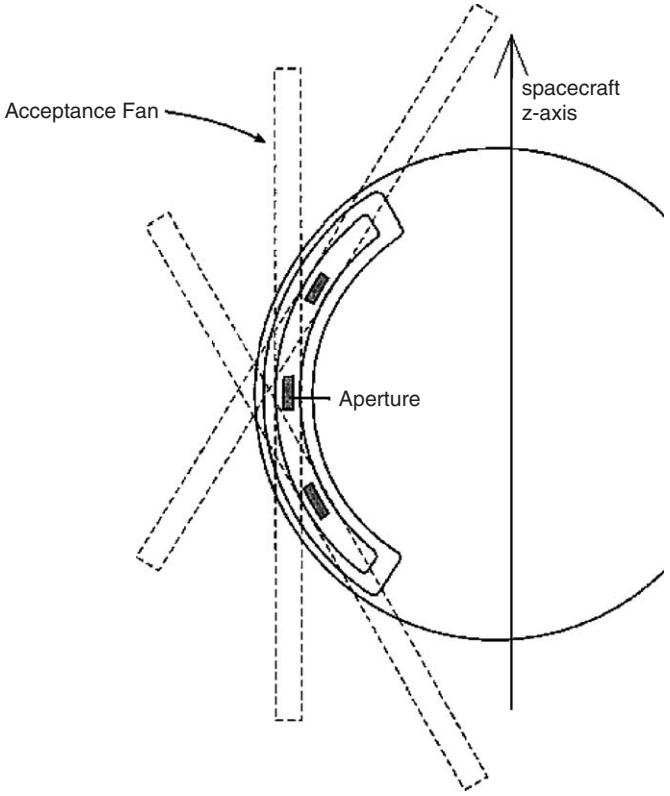

Fig. 2. The crossed-fan viewing geometry of IBS. There are three curved 2.5×15 mm apertures in the IBS faceplate, each with a nominal acceptance fan of ±1.5° in azimuth and ±75° in elevation (set by the apertures) from the normal to the plane of the aperture. If we define the middle aperture as being along the 0° radius from the center of the faceplate, the other two apertures are located at ±30° relative to it. The field of view (FOV) of the middle aperture is oriented such that its long (polar) dimension is parallel to the azimuthal rotation axis of the CAPS actuator. The FOV of the other two apertures are therefore "crossed" with inclinations of ±30° with respect to that of the middle aperture. The spacecraft z-axis is in the plane of the figure, its orientation is also shown; this is perpendicular to the rotation plane of the actuator. The angle in the rotation plane, relative to the $-y$-axis is called azimuth; the inclination angle of a given direction to the rotation plane is elevation.

Below we present magnetic field data in a frame aligned with the shock normal, defined by the direction of the minimal and maximal field variations (Sonnerup and Scheible, 1998), and all the rest of the plasma data in the SCRS.

3. Data analysis

From now on we shall denote time in fraction of hours instead of the hour:min form, because it is more convenient for the analysis. At the outset we have to note the plasma data measured in the foot between 8.75 and 10.5 UT have several limitations. The time resolution of the magnetic field is low (24-s), and CAPS–IBS resolves energy only. Consequently, we are unable to characterize fully the plasma; our approach will be to set up a model for the phenomena we investigate, and we analyze whether the measured parameters fit into the framework of the model. In some cases we have to make assumptions; a crucial one is the magnitude of the velocity of the solar wind perpendicular to the shock front, $\mathbf{v}_{SW\perp}$. To assess this we use the geometry shown in Fig. 1, which indicates that the angle between the Sun direction and the Joy et al. (2002) model BS normal is $\sim 75^\circ$. As defined using the method described in Sonnerup and Scheible (1998), the shock normal in the JSEQ system was (0.244, 0.963, −0.118), giving an angle of about 76.3° with the Sun direction. Assuming that the solar wind direction is close to the Sun direction, we shall assume in the model calculations that $\mathbf{v}_{SW\perp}/\mathbf{v}_{SW||}$ is about 0.2–0.25 where $\mathbf{v}_{SW||}$ is the velocity component of the solar wind parallel to the BS.

The shock normal direction was inclined to the average magnetic field vector by about 5° (the actual value of this angle is somewhat sensitive to the time interval we use to define the shock normal direction); hence, this BS was a quasi-parallel shock. In the SCRS the shock normal is close to the z-direction (c.f. Fig. 1.); the average magnetic field between 9.0 and 10.5 UT was $\mathbf{B}_{av} = (-0.011, 0.152, 1.08)$ nT in the SCRS, so $|\mathbf{B}| \sim 1.1$ nT; its orientation in JSEQ is also shown in Fig. 1.

Our interpretation of this plasma event is based on the theory developed by Quest (1988) for quasi-parallel shocks. In this model, a portion of the impinging solar wind is reflected by the magnetic structures formed downstream, reappearing upstream as a counter-streaming beam in the solar wind. The reflected particles gyrate around the magnetic field. Because of the large angle between the shock normal and the solar direction, the incoming solar wind particles have a high velocity component parallel to the shock front $\mathbf{v}_{SW||}$, and a much smaller component perpendicular to it. When these particles cross the shock, they retain the parallel velocity $\mathbf{v}_{SW||}$, and their perpendicular velocity decreases. In the frame that is co-moving with $\mathbf{v}_{SW||}$, some particles are reflected back by downstream magnetic fluctuation; an individual reflected particle will have a velocity $\mathbf{v}_1$ parallel to $\mathbf{B}$ (causing the backstreaming), and $\mathbf{v}_2$ perpendicular to $\mathbf{B}$, resulting in the gyration. The reflected particles in the foot are visualized as a ring in velocity space, backstreaming along the magnetic field with a guiding velocity given by the average of the $\mathbf{v}_1$ velocities, and perpendicular to $\mathbf{B}$ given by $\mathbf{v}_2$. As $\mathbf{B}$ is parallel to the shock normal, and in this model the solar wind flows along the shock normal, the beam can propagate far upstream (order of 10 Larmor radii), creating a very perturbed foot. In what follows we shall show that it is plausible that the backscattered particles excite a nonresonant fluid instability, the firehose instability. This instability can transfer the free energy of the backscattered particles and the Alfven waves present in the foot to the solar wind to accelerate it. When the firehose instability cannot be excited, the solar wind plasma returns the energy, and slows down. The repetition of this process produces the observed velocity excursions of the incoming solar wind beam. We describe this in more detail in Section 4.

In this section we discuss the different plasma features observed in the shock foot. In Fig. 3 we present an overview of the plasma history, including the solar wind velocity spectra both for protons and α particles, the measured values of the total magnetic field and its components in the minimum variance frame of reference, and the electric field power spectra between 6.0 and 11.0 UT.

The solar wind spectra shown in Fig. 3 were collected by the middle sensor of CAPS–IBS, and the electric field between 1 Hz and 10 kHz was measured by RPWS. The solar wind was still unperturbed after 6.0 UT; its velocity was quite stable, ~430 km/s, and the thermal velocity ($v_T \sim \sqrt{2T/m_p}$) was 8–10 km/s. The solar wind velocity started to decrease slowly at about 7.0 UT. Strong fluctuations appeared at about 8.35 UT, by chance at almost the same time that the spacecraft orientation changed. After that the bulk α and proton velocities reached the unperturbed solar wind velocity for short periods, but never exceeded it. The spacecraft crossed the BS at about 10.5 UT. This is clearly indicated by the strong wave signature and the onset of the ion heating; the ion thermal velocity exceeded 50 km/s downstream. In the downstream region the bulk plasma velocity stabilized at 370–380 km/s around 12.0 UT (not shown in the figure). The BS is a typical quasi-parallel shock: B_{tot} is almost unchanged as we cross the shock. Strong short-period waves are superimposed on the magnetic field, making it turbulent. A very important feature of the incoming flow is that the protons and the α particles fluctuate together. In the kinetic mode of wave particle interactions only a part of the distribution function resonates with the waves; however, when the interaction is of fluid type, a macroscopically significant portion of the distribution is in resonance with the waves. In this latter case the bulk velocity of the distribution function also strongly reflects the interaction. Therefore if we see that the bulk velocity both of the protons and the alphas are behaving in a similar way, it indicates that we have a fluid-type instability organising the interaction between the incoming beam and ions reflected

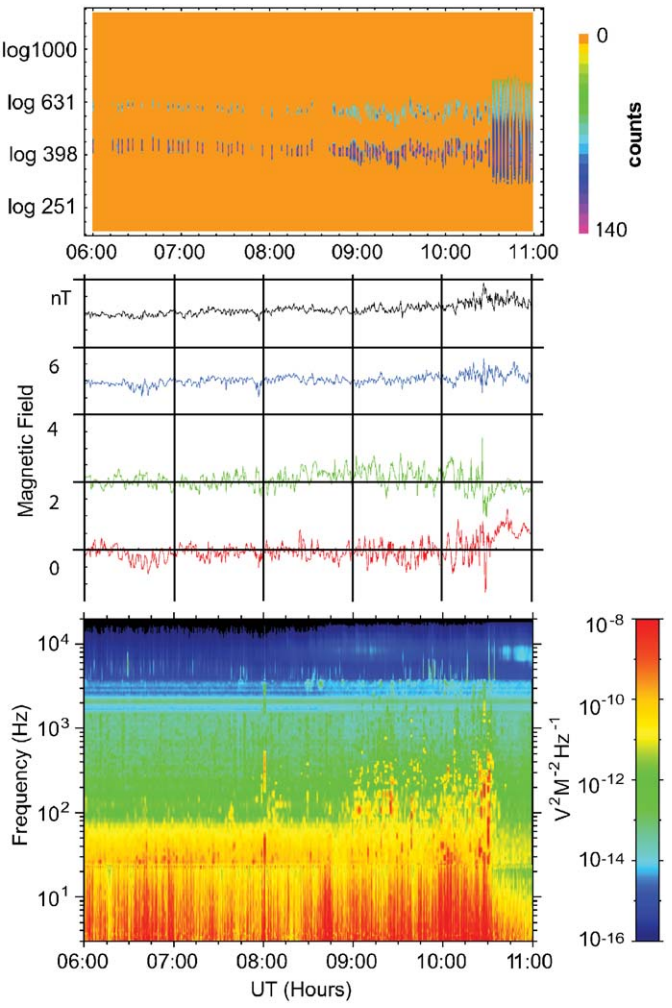

Fig. 3. *Top panel*: color-coded, linear count rate spectra of the solar wind plasma, plotted as a function of log velocity in km/s units (vertical axis), and time (the velocity of the α particles is $1/\sqrt{2}$ of the indicated values). The horizontal axis is time in UT between 0600 and 1100 in all three plots. The banded structure is due to the actuator motion because the solar wind was not always in the field of view. The upper band exhibits the α particles and the lower band shows protons. *Middle panel*: Magnetic field data in the minimum variance frame. The minimum variance direction is marked blue, and is shifted up by 4 nT; the maximum variance direction is red, and the intermediate direction is green, shifted upwards by 2 nT. B_{tot} is black, shifted upwards by 6 nT. *Lower panel*: The color-coded intensity of the measured waves (in dB above background), plotted as a function of log frequency.

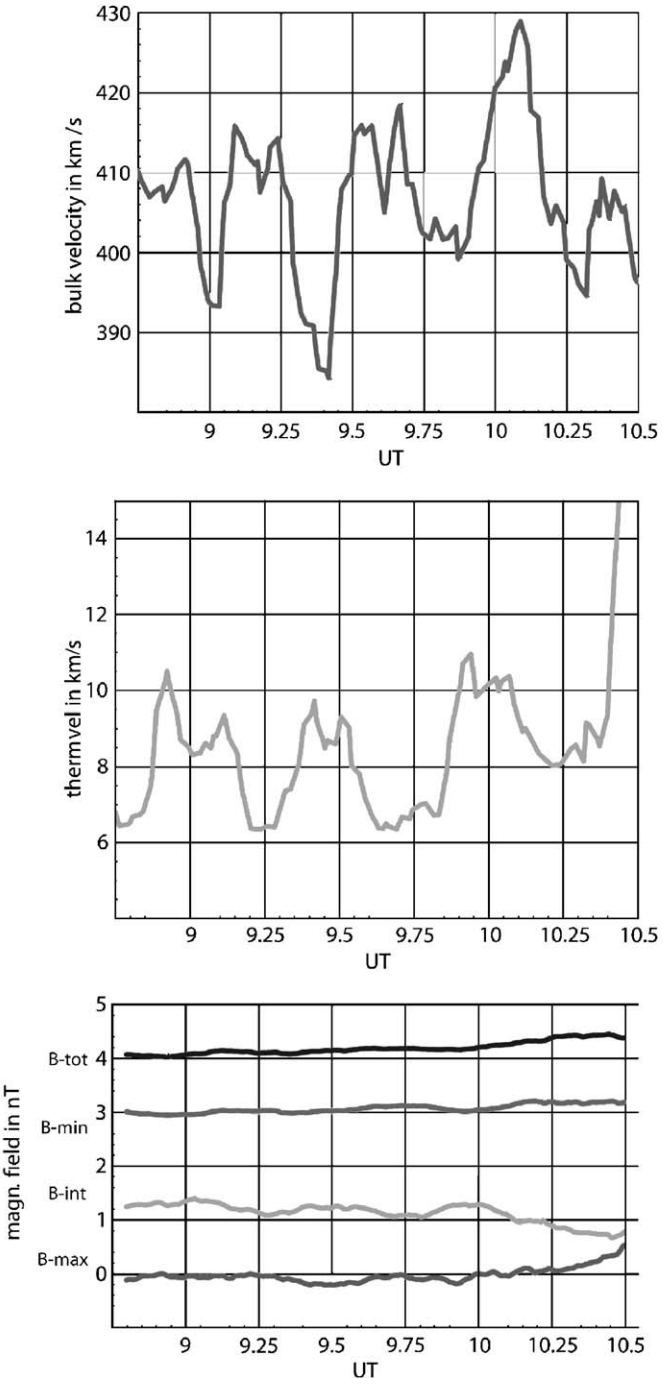

Fig. 4. The proton bulk speed (upper plot), and the thermal velocity (middle plot) in km/s are shown as a function of time measured by the middle sensor of IBS. The data shown were smoothed, by a 160-s-long moving average. The bottom plot shows long-wavelength waves in the magnetic fields. From top to bottom: B_{tot}, next is the field component along the shock normal B_{min}, then B_{int}, and B_{max} shifted up by 3, 2, 1, and 0 nT, respectively. See text for further details.

from behind the shock front. We argue in Section 4 that this is a firehose instability.

We have derived bulk proton parameters using the measured IBS spectra by fitting single Maxwellians. The bulk speed and the thermal velocity for the middle sensor of IBS are shown in the two upper plots of Fig. 4. The bulk speeds determined from the other two IBS sensors are the same, but there are variations in the thermal velocity. Fig. 4 shows a certain anticorrelation between the bulk and thermal velocities. Between 9.04 and 9.1 UT the proton bulk speed changed by $\sim$40 km/s, corresponding to $\sim$130 ms^{-2} average acceleration of the bulk speed.

We turn to the analysis of the individual proton spectra measured by IBS. The simplified geometry of the measurement is exhibited in Fig. 5. We use here the assumption that the solar wind has a high velocity component parallel to the shock surface, and a much lower component

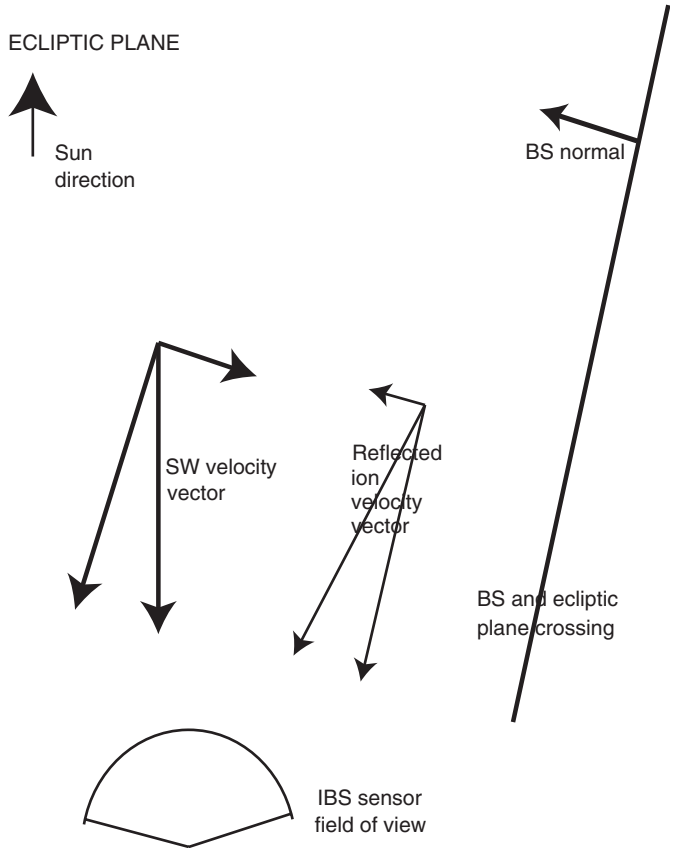

Fig. 5. The simplified geometry of the IBS data collection is shown in the ecliptic plane, in the spacecraft frame of reference. The bow shock is represented by a plane perpendicular to the ecliptic; both the solar wind and the average reflected beam velocities are displayed. The IBS middle fan rotates 12° above and 43° below the ecliptic plane. This simplification neglects the small inclination of the IBS rotation axis to the ecliptic plane.

($\sim$0.2–0.25$\mathbf{v}_{SW||}$) perpendicular to it. As discussed above as well, when the solar wind crosses the shock front, the parallel component should be unchanged while the perpendicular component is decreased. If the solar wind particles are reflected back upstream, in the spacecraft frame their distribution is a ring-beam drifting with $\mathbf{v}_{SW||}+\langle \mathbf{v}_1 \rangle$ spread by $\langle \mathbf{v}_2 \rangle$; where $\langle\ \rangle$ denotes averaging. That is, the magnitude of the velocity of the reflected population should be close to the shocked bulk plasma speed, 370–380 km/s. In reality the backscattered particles are also spread in velocity space due to the velocity spread of the scatterers; this distorts the ring-beam, hence their actual distribution in the spacecraft frame of reference is very likely close to a broad Maxwellian centered on a velocity lower than that of the bulk solar wind velocity. Because the actuator axis of IBS is almost parallel to the ecliptic plane, both the incoming solar wind and the reflected beam are within the field of view of the middle sensor, and therefore both populations contribute to the observed energy spectra shown in Fig. 3.

In the foot of the shock the proton distributions generally are quite perturbed and variable. In Fig. 6 we present proton distributions as measured by the middle sensor of IBS near the minimums and maximums of the bulk velocity shown in Fig. 4. The upper plots were measured between 09.035 and 09.09 UT, the next below between 9.24–9.36, 9.38–9.51, and 9.62–9.67, respectively. (The distributions are ordered by bulk velocity and not by time, because of the windshield-wiper-like motion of the actuator.) The dots are the measured values, the continuous lines are Maxwellians fitted to the central part of the distributions. Corresponding to the physical picture explained above, we identify the deviations from the Maxwellian shape as the proof of reflected protons. The reflected populations appearing at lower/higher energies effectively broaden the distribution function, causing an increase in the apparent thermal velocity. Hence, we interpret the thermal velocity changes exhibited in Fig. 4 as an indication of the variable amount of reflected particles in the foot. The density of the reflected ions may reach $\sim$30% of the solar wind density, e.g. in the upper middle plot. The thermal velocities measured in the other sensors in some cases differ from the values measured by the middle sensor. We interpret such cases as an indication that the temperature of the solar wind becomes anisotropic. Strong reflected population is generally accompanied by an anisotropic thermal distribution in the range of $v_T\sim$7–13 km/s as measured by the three fans. In Fig. 6 we do not see strong indications for reflected ions when the bulk velocity is high. The analysis supports a picture in which a dense-reflected population appears when the bulk velocity of the solar wind is low, with lower density at higher solar wind bulk velocity in the foot. The reflected ions apparently follow sort of a burst-like pattern, and most of the time they are present with variable density.

The pattern we infer from Fig. 6 is that solar wind acceleration is accompanied by higher reflected beam densities (hence with higher effective temperature), and we shall show later that these cases allow the excitation of the firehose instability. The instability operates until the reflected beam density becomes low again. The cause of the burst-like nature of the reflected population is unknown.

The angular width (defined as $\arctan(v_{thermal}/v_{bulk})$) of the solar wind distributions is about 4° ($v_{thermal}$ taken at two counts level), the width of the reflected distribution is less than 8°, in all of the three fans. This narrow angular width is the reason that when the IBS sensors loose the solar wind rotating away from the ecliptic plane, in general they also loose the reflected beam.

According to *Quest's* model, the reflected particles could excite either firehose instability or cyclotron resonances. The dispersion relation for the impinging solar wind and counter-streaming ion beam is given in Eq. (3) of Quest (1988). First we show, that the excitation of the non-resonant firehose instability in the foot is possible. Its condition, as given by Eq. (21) of Quest (1988) is that ω/k should be pure imaginary,

$$\frac{\omega}{k} = V_A\sqrt{1-\frac{\beta_{par}-\beta_{perp}}{2}-\eta(1-\eta)U^2}, \quad (1)$$

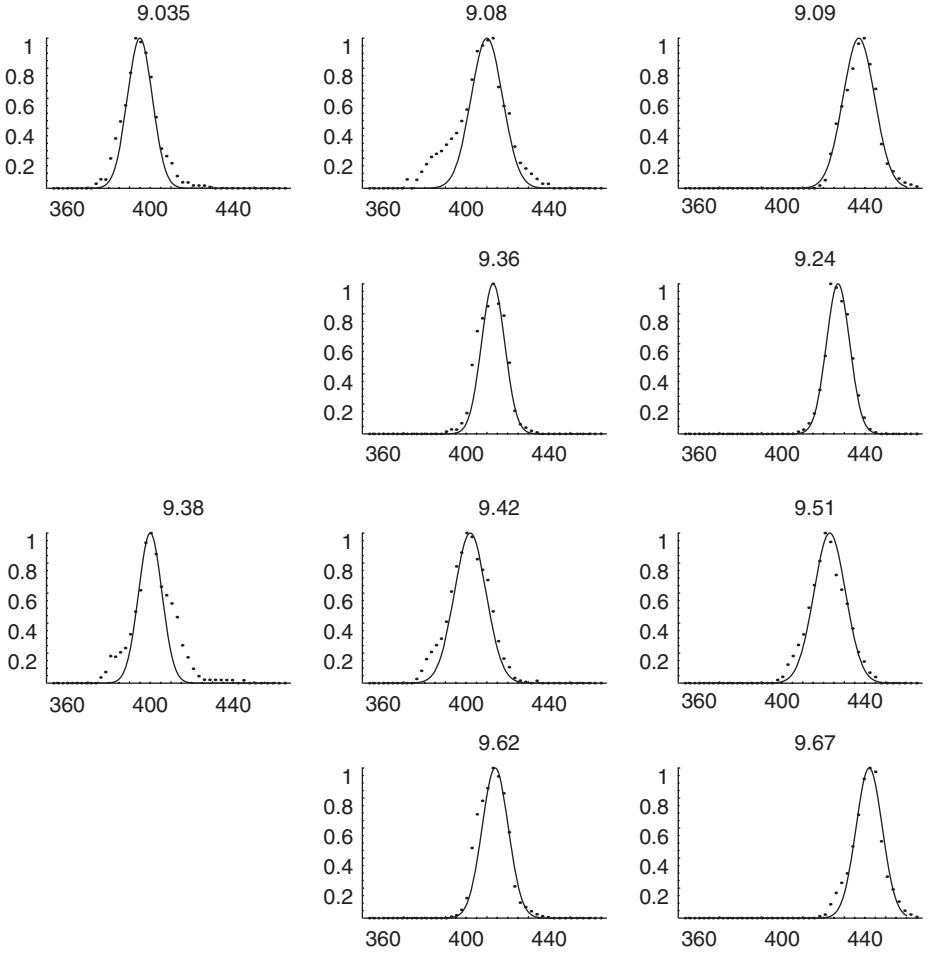

Fig. 6. Proton distributions measured by the middle channel of IBS. The horizontal axis shows velocity in km/s; the vertical axis is in arbitrary units. In each plot the time of measurement is given in UT (all these distributions were measured between 9.0 and 10.0 UT); near the minima and maxima of the bulk speed shown in Fig. 4. The dots are the measured values; the continuous lines are Maxwellians fitted to the central part of the distributions.

where ω is the wave frequency, k is the wave vector, η is the density ratio of the reflected protons to the impinging solar wind, V_A is the Alfven velocity, U is the relative velocity of the solar wind and the reflected ions in the direction perpendicular to the BS front, normalized to V_A; β_{par} and $_{perp}$ are the ratios of the parallel and perpendicular thermal pressure to the magnetic pressure, respectively. The last term under the square root in Eq. (1) is due to the contribution of the relative drift to the parallel pressure. From the data presented above we can assess the magnitude of the terms under the square root.

The Alfven velocity for $B = 1.1$ nT and $n = 0.34$ particle/cm^3 (we assume that the density measured by ELS is characteristic of the solar wind density) is $V_A = 41$ km/s. In most of the cases studied in the literature the firehose instability is driven by the difference between the parallel and perpendicular components of the thermal pressure. In our case the difference of the plasma β terms is of the order of 0.1 as it can be seen from the temperature values presented in Fig. 4., i.e. it is too low to drive the instability. However, the last term under the square root, the contribution of the relative drift motion to the parallel pressure provides the required pressure anisotropy. The reflected beam density is not constant in the foot; we have shown examples in Fig. 6 when the density was about 30% of the solar wind density, whereas in other cases it was much lower. To assess the solar wind velocity perpendicular to the BS first we recall that the upstream solar wind velocity, as can be seen from Fig. 3., is about 400–420 km/s. We argued using the geometry shown in Fig. 1 that $\mathbf{v}_{SW\perp}/\mathbf{v}_{SW||}$ is about 0.2–0.25. Hence the upstream proton flow velocity perpendicular to the shock front, before the foot is about 2–2.5 V_A; that is this velocity is about 80–100 km/s (c.f. Fig. 3.). In the foot this speed is modulated by about 1 V_A. The parallel speed of the reflected beam is lower than that of the solar wind; obtaining its value from the difference between the upstream and downstream bulk velocity shown in Fig. 3, it is lower by about one V_A. Consequently, U in Eq. (1) can be about 3–4 since the beams are counter streaming. Taking into account the observed values for η, in such cases the onset of the firehose instability is possible, because $\eta(1-\eta)U^2$ can be significantly greater than 1. (We remind the reader it was shown before that η was high when the bulk flow velocity in the

foot was low.) Though our measurements do not allow us to get an exact value for Eq. (1), as an order-of-magnitude assessment the growth rate is $\sim kV_A$.

Because of the one-dimensional nature of our plasma measurements we are unable to test the resonance conditions of the cyclotron resonances directly. However, we could have looked whether there are evidences of the cyclotron instabilities, because in many other cases they are good indicators of reflected particles. In our data, we could not find the cyclotron resonances using the conventional techniques. We should note that this does not fully exclude their presence, because in our case, due to the variable plasma conditions and firehose excitations the cyclotron resonance excitation should follow a pattern varying in time. The cyclotron resonance frequency for protons in a magnetic field of 1.1 nT is 0.0167 Hz. In the case when the electromagnetic instabilities are excited by relative drift motion of beams, the resonance frequency depends on the drift velocity as well, and it is shifted by ku_{drift}, where k is the wave number, and u_{drift} is the drift velocity (in linear approximation this is discussed e.g. by Ichimaru (1973); or see the discussion of Eq. (3) in the paper of Quest (1988)). We have shown above that the velocity of the solar wind varies by about 40 km/s in $\mathbf{v}_{\mathrm{SW}\perp}$ (Fig. 4), but we do not know the variation of the beam velocity. An additional complication is the variable density of the reflected ions. Therefore, even in the case where the linear approximation is a proper description of the plasma, we cannot expect sharp peaks in the Fourier spectra of the magnetic fields; the resonance frequency of the cyclotron resonance is smeared due to the variable drift velocity. The fact that the cyclotron resonances are probably not always present in the foot further diminishes their signature in the Fourier spectra. Furthermore, the magnetic field in the foot is turbulent, i.e. very strongly perturbed; this means that we are not in the linear regime. Accordingly the individual Fourier components do not develop in time independently from other components (even in the absence of the smear discussed above), and the amplitude of the Fourier components might depend on time. Hence we cannot analyse the cyclotron resonances in the same way as in the linear theory; the strong variation of $|\Delta\mathbf{B}|$ destroys the usual "circular shape" of the hodograms, and both the smear of the resonance frequency and the turbulence affect the time variation of the phase angle.

To find longer-period magnetic waves we smooth the magnetic field data using a 10-min-long window; the result is exhibited in the lower plot of Fig. 4. The magnitude of wave amplitudes (except the vicinity of the BS), if cleansed from the background, is reasonably constant, as required for Alfven waves. The waves, superimposed on a constant background, propagating almost parallel to the minimum variance direction, the variations of the field vectors is nearly perpendicular to it. Therefore, we believe that these are Alfven waves. The wave period is about 20 min in the SCRS. The reflected particles might excite these Alfven waves as discussed in Kennel et al. (1985), and Szego et al. (2000). The Alfven waves are loosely correlated with the solar wind velocity changes as can be seen in the figure.

We continue the analysis with the electron data. CAPS–ELS and MAG data have been used to plot electron pitch angle distributions for the period 9.16–11.0 UT 30 January 2001. These data are shown in Fig. 7 for electron energies of 0.05–1 keV with a time resolution of 128 s (64 energy sweeps). For each measurement the pitch angles covered by each anode are calculated using 1-min. magnetic field measurements from MAG. Each row represents the differential energy flux measured in one ELS energy channel. Fifteen 12°-wide pitch angle bins are used, with 0° pitch angle at the bottom and 180° at the top. For further information on the details of this plotting technique see Abel et al. (2001). The core (or thermal) solar wind component and photoelectrons are generally below ~20 eV, and are not shown here as the scale has been selected to show the more sparse higher energy electrons. After the BS crossing at ~10.5 UT the heated and compressed core electrons are in the region of saturation of the ELS sensor, between 20 and 200 eV.

From the beginning of this plot until the shock crossing there is a population of counter-streaming electrons from 0.05 to 26 keV (the highest energy measured by ELS); the incoming solar wind and the reflected electrons. The observed energy and spectral shape is consistent with these being foreshock particles, which may be found upstream of a quasi-parallel shock. These have been observed at energies between 0.01 and 30 keV (Fitzenreiter, 1995, and references therein). It seems likely that we are observing two populations at this time: one of counter-streaming electrons which may be related to the electron foreshock and superposed on this a population of electrons above 0.8 MeV manifest in the ELS data as penetrating radiation at all energies with no pitch angle dependence. Interestingly we continue to observe relatively energetic counter-streaming electrons in the magnetosheath; these are probably also shock-accelerated electrons.

Electron density of the core component of the upstream solar wind at this time was approximately 0.34 particles cc^{-1} and the electron temperature was just above 3 eV. Details of the derivation of these values are given in a survey of the up/downstream electron parameters at each of the Cassini BS crossings by Rymer et al. (2006). The frequency of the Langmuir waves observed near 6 kHz in Fig. 3 independently gives a solar wind density of about 0.44 cm^{-3}.

It was suggested first by Moses et al. (1984) that hot electrons backstreaming from the shock excite electrostatic waves in the frequency range 100–1000 Hz, as observed during the Voyager mission. We display in Fig. 8 similar waves observed by RPWS in the foot region of Jupiter; we believe that these wave features in the foot correspond completely to the model of Moses et al. (1984).

Up to this point we have assumed that the BS we encountered was a stable BS. Last we investigate what might happen when this might not be the case; whether

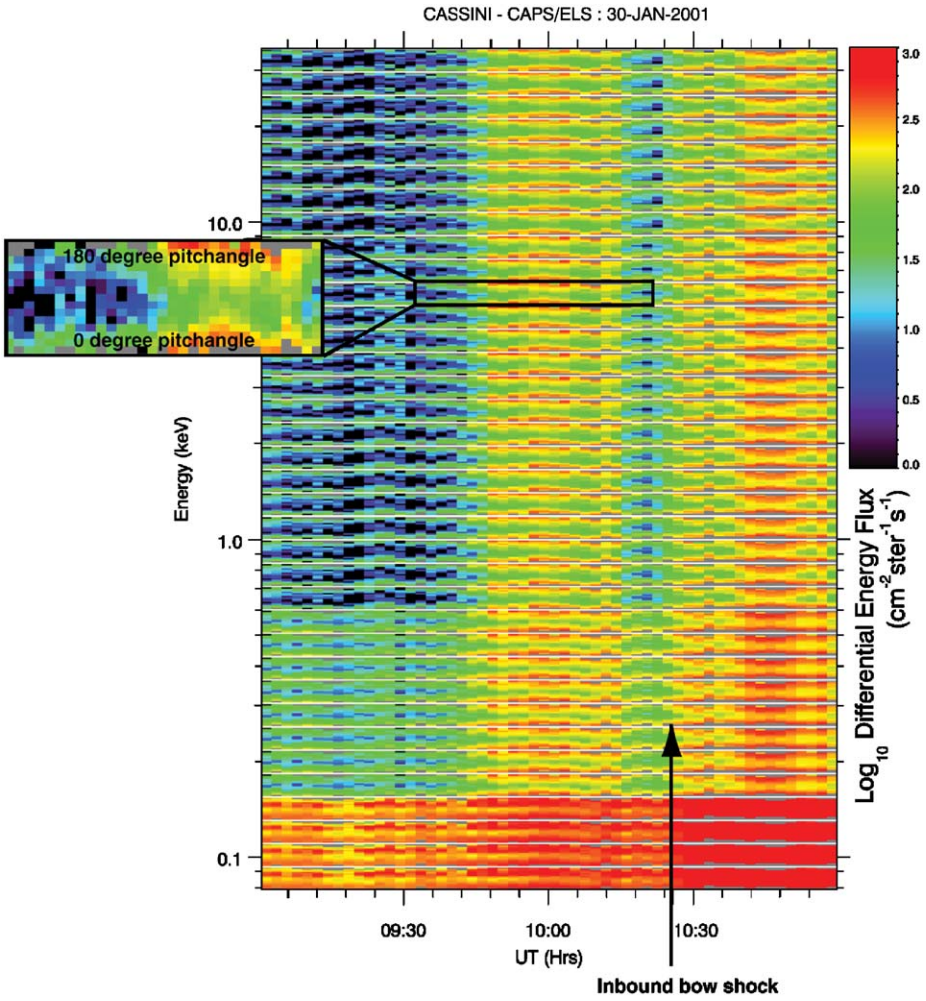

Fig. 7. CAPS–ELS electron pitch angle distributions, 30 January 2001, 0900–1100 UT. Each band (separated by a white line) corresponds to one ELS energy channel as shown on the y-axis. Within each band the pitch angle distribution is shown from 0° at the bottom to 180° at the top; one channel is enlarged to exhibit better the backstreaming electron flow. Both the incoming SW particles and the reflected ones are shown. Differential energy flux is indicated by the color bar. See text for further details.

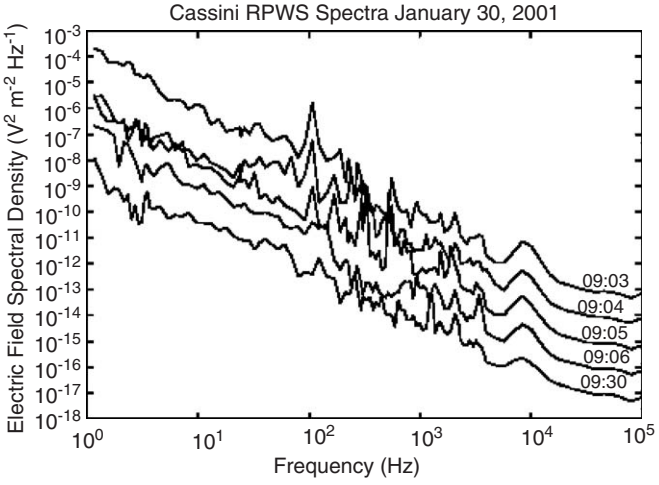

Fig. 8. Spectral density of the electric field measured by RPWS at 0903, 0904, 0905, 0906, and 0930 UT. The spectra are multiplied by ten, consecutively.

other explanations could reproduce the observed plasma features. It is known from the literature (Omidi and Winske, 1990) that shocklets can develop at low Mach numbers, and this can modify the plasma in the foot. To this end, we have examined whether shocklets could have been formed in the given region, and if the answer is affirmative, what are the plasma features predicted.

We did a simulation run using a hybrid code described in Bagdonat and Motschmann (2002a, b). Up to now it seems impossible to resolve small scale features for the Jovian BS when doing a quantitatively correct global simulation, so this result serves as a simple model to illustrate the basic physical properties occurring at a quasi-parallel shock.

To generate the shock, a simple fixed ionospheric obstacle was used rather than a magnetospheric obstacle, which should not make any difference. The simulation is 2D with the magnetic field lying in the simulation plane, and forming an angle of 60° with the solar wind flow

direction (x-direction). The Alfven Mach number was chosen to be 3. We chose this very simple geometry and parameters because in this configuration the effects we want to demonstrate are more pronounced. These results may be compared to similar ones given in Shimazu (2001) and Omidi et al. (2001). From the simulation results we conclude that it is less likely that shocklet formation can explain the observations; however, the presence of circularly polarized Alfven waves in the foot region in the simulation is consistent with the firehose instability interpretation.

4. Conclusions

In this paper we have investigated the foot region of an almost parallel shock Cassini encountered on 30 January 2001, at 1030 UT. The craft at the beginning of that day was at a distance of $424.5R_J$ ($1R_J = 71,492$ km) from Jupiter, $\sim 47^\circ$ behind the terminator line in JSEQ, and $\sim 0.5^\circ$ below the equatorial plane, on the dusk side of the planet (c.f. Fig. 1). The most striking feature was that before the BS crossing, the incoming solar wind first decelerated, than the bulk velocity both of the proton and α components increased; the flow accelerated and decelerated, heated and cooled several times. In this paper we have attempted to provide an explanation for this. As we have mentioned in the introduction, another important feature of this event is that the combination of field geometry, flow direction, and shock orientation allows the shock front to extend well in front of the shock. The shallow crossing angle of the spacecraft with respect to the foot allows its features to be sampled over hours rather than minutes.

Our baseline was the model of Quest (1988); according to that model at parallel shocks there appears a reflected beam that can propagate far upstream creating a very perturbed foot. We note that Quest's model is one-dimensional, but describes surprisingly well the real situation in the foot.

The shock normal was almost parallel to the upstream average magnetic field vector; therefore, this was a quasiparallel BS event. In the upstream solar wind the plasma β was low, ~ 0.1, and in the direction parallel to the shock normal the Mach number was also low. We have interpreted the behavior of the incoming solar wind as the result of its interaction with waves excited by the particles reflected from behind the shock front. We have argued that the interaction has lead to firehose instability. The burst-like behavior of the reflected beam results in the variable slowing. We cannot explain why the reflected beam is so variable in time. We investigated another possible mechanism, namely whether shocklet formation could account for the observations. Whereas shocklet formation at low Mach number shocks reproduces well the velocity and thermal variations, the other observed and predicted plasma parameters differ. Therefore we have concluded that this scenario is less likely.

The reflected energetic electron population is responsible for the waves measured in the 100–1000 Hz frequency interval, confirming the Voyager observations.

Most of the BS crossings observed by Cassini were quasiperpendicular; but there are a few quiasiparallel crossings as well. In those cases there are also some evidence for the excitation of firehose instability, but those are not as pronounced as the case examined here.

Acknowledgements

The support of K. Sz. by OTKA T-32634 Grant is acknowledged. The research at The University of Iowa was supported by NASA through Contract 961152. Work at Los Alamos was conducted under the auspices of the US Department of Energy, with support from the NASA Cassini program.

Appendix A. Modeling the velocity excursions of the solar wind in the foot

In this section we asses using a simple 2-D model how big the velocity excursion can be in the foot region, if the excursion is related to firehose instability. We show within this simplified framework that the amount of free energy available in the foot can be adequate for the acceleration of the incoming beam, but we could not provide a detailed analysis as to how the firehose instability mediates the energy transfer. Accepting the estimate given in Section 3 that the growth rate is $\gamma/k \sim V_A$, we can give a crude estimate of the acceleration of the flow, following the considerations of Arcimovich and Sagdeev (1979). In that simple picture, the particles are gyrating along the curved field lines of the Alvfen waves. Firehose resonance develops when the centrifugal forces along the curved sections are not balanced by other forces. In such cases the acceleration (perpendicular to the average magnetic field direction) is given as the time derivative of the plasma drift velocity,

$$\frac{dv}{dt} = \frac{d}{dt} c \frac{E}{B_0} = \int d\omega \exp(i\omega t)(i\omega) c \frac{E_\omega}{B_0} = \int d\omega \exp(i\omega t) \frac{\gamma^2}{k} \frac{B_\omega}{B_0} \sim \frac{\gamma^2}{k} \frac{B}{B_0}, \quad \text{(A.1)}$$

where B is the magnitude of the magnetic field of the Alfven waves, B_0 is the average background magnetic field value (c.f. Fig. 4c), E_ω and B_ω are the Fourier components of the electric and magnetic fields, respectively. We used the Maxwell equation $\nabla \times \mathbf{E} = -(1/c)(\partial \mathbf{B}/\partial t)$, and $i\omega = \gamma$ for the firehose instability; we assumed that the Fourier spectrum is centered on the Alfven waves.

To assess the wavelength of the Alfven waves we use the same estimate for the solar wind velocity perpendicular to the shock front as above; that is, this velocity is about 80–100 km/s. The Alfven waves we are talking about—if excited by the reflected particles—propagate away from the

shock (c.f. Kennel et al., 1985). This means that the waves pass the spacecraft with a velocity of about 40–60 km/s; that is during the observed 20 min period their wavelength is about 50,000 km, or $1/k \sim 10^4$ km. In our case $B/B_0 \sim 1$, hence Eq. (A.1) gives $\mathrm{d}v/\mathrm{d}t \sim 100 \div 150\,\mathrm{ms}^{-2}$, in a surprisingly good agreement with the measured bulk speed variation.

The exact analysis of the energy transfer via firehose instability in the foot, between the solar wind on one hand and the reflected beam and Alfven waves on the other, is a very difficult problem, and in most of the cases it requires nonlinear approximations and numerical simulations, as is shown in Gary et al. (1998), and Quest and Shapiro (1996). In this paper we do not attempt to discuss it in details.

In the rest frame of the solar wind the energy sources are the free energy of the reflected beam and the Alfven waves (excited by the beam). The wave energy density W_{E} for Alfven waves can be approximated as $H^2/4\pi$, because the electric field energy density W_{ele} is equal to the magnetic field energy density:

$$W_{\mathrm{ele}} = \int \mathrm{d}k \frac{\partial(\omega\varepsilon_k)}{8\pi\partial\omega} E_k \bar{E}_k \sim \frac{c^2}{V_{\mathrm{A}}^2 8\pi} \frac{|H_k|^2\gamma^2}{k^2c^2} \Delta k = \frac{1}{8\pi}|H_k|^2\Delta k \sim \frac{1}{8\pi}H^2. \quad (A.2)$$

Here ε_k is the dielectric constant, the bar denotes complex conjugate; Δk is the interval around the wave vector k where the Fourier spectra of the fields are centered, H_k and E_k are the Fourier components of the fields in spatial variables. The value of ε_k can be assessed for propagation parallel to the magnetic field from the refractive index n, because $\varepsilon_k = n^2 = k^2\, c^2/\omega^2 \sim c^2/V_{\mathrm{A}}^2$ (see e.g. Stix (1992), or Arcimovich and Sagdeev (1979)); k is the magnitude of the wave vector and c is the speed of light. If H_k is centered on a small interval in k as we have already assumed, its Fourier transform is almost constant. Therefore, we could take advantage of the Parseval theorem for Fourier transforms (assuming unit volume) to obtain the last part of Eq. (A.2).

Hence $W_{\mathrm{E}} \sim 10\,\mathrm{eV\,cm}^{-3}$. This means that the energy density of the Alfven waves alone would be sufficient for the acceleration of the solar wind, because the observed increase of the particle energy density in the solar wind frame of reference is

$$n_{\mathrm{p}} \frac{1}{2} m_{\mathrm{p}} \Delta v^2 \approx 4.5\,\mathrm{eV\,cm}^{-3}, \quad (A.3)$$

where $n_{\mathrm{p}} \sim 0.34$ is the proton density we used above, m_{p} is the proton mass, and $\Delta v \sim 40$ km/s is the measured change of the bulk plasma speed.

These processes conserve entropy, that is the energy accumulated in the waves and particles can be exchanged freely. Therefore, when the firehose instability is damped, the plasma flow in the foot may return its energy to the other plasma components.

References

Abel, G.A., Coates, A.J., Rymer, A.M., Linder, D.R., Thomsen, M.F., Young, D.T., Dougherty, M.K., 2001. Cassini observations of bi-directional lobe electrons during the earth fly by, 18th August 1999. J. Geophys. Res. 106, 30,199–30,208.

Arcimovich, L.A., Sagdeev, R.Z., 1979. Plasma Physics for Physicists. Atomizdat, Moscow (in Russian).

Bagdonat, T., Motschmann, U., 2002a. 3D hybrid simulation code using curvilinear coordinates. J. Comput. Phys. 183, 470–485.

Bagdonat, T., Motschmann, U., 2002b. From a weak to a strong comet—3D global hybrid simulation studies. Earth, Moon and Planets 90, 305–321.

Dougherty, M.K., et al., 2004. The Cassini magnetic field investigation. Space Sci. Rev. 114, 331–383.

Engel, I.M., Beard, D.B., 1980. Idealized Jovian magnetopause shape and field. J. Geophys. Res. 85, 579.

Fitzenreiter, R.J., 1995. The electron foreshock. Adv. Space Res. 15, 9–27.

Gary, S.P., Li, H., O'Rouke, S., Winske, D., 1998. Proton resonant firehose instability: temperature anisotropy and fluctuating filed constraints. J. Geophys. Res. 103, 14,567–14,574.

Gurnett, D.A., et al., 2004. The Cassini radio xand plasma wave investigation. Space Sci. Rev., in press.

Huddleston, D.E., Russell, C.T., Kivelson, M.G., Khurana, K.K., Bennett, L., 1998. Location and shape of the Jovian magnetopause and bow shock. J. Geophys. Res. 103, 20,075.

Ichimaru, S., 1973. Basic Principles of Plasma Physics. Benjamin Publishing Co., London.

Joy, S.P., Kivelson, M.G., Walker, R.J., Khurana, K.K., Russell, C.T., Ogino, T., 2002. Probabilistic models of the Jovian magnetopause and bow shock locations. J. Geophys. Res. 107 (A10), 1309.

Kennel, C.F., Edmiston, J.P., Hada, T., 1985. A quarter century of collisionless shock research. In: Stone, R.G., Tsurutani, B.T. (Eds.), Collisionless Shocks in the Heliosphere: A Tutorial Review. AGU Geophysical Monograph 34, pp. 1–36.

Linder, D.R., Coates, A.J., Woodliffe, R.D., Alsop, C., Johnstone, A.D., Grande, M., Preece, A., Narheim, B., Svenes, K., Young, D.T., 1998. The Cassini CAPS electron spectrometer. In: Pfaff, R., Borovsky, J., Young, D. (Eds.), Measurement Techniques in Space Plasmas: Particles. AGU Geophysical Monograph 102, pp. 257–262.

Moses, S.L., Coroniti, F.V., Kennel, C.F., Scarf, F.L., 1984. Strong electron heat flux modes in Jupiter's foreshock. Geophys. Res. Lett. 1, 869–872.

Moses, S.L., Coroniti, F.V., Kennel, C.F., Kurth, W.S., Gurnett, D.A., 1990. Comparison of plasma wave measurements in the bow shocks at Earth, Jupiter, Saturn, Uranus and Neptune. Geophys. Res. Lett. 17, 1653–1656.

Omidi, N., Winske, D., 1990. Steepening of kinetic magnetosonic waves into shocklets: simulation and consequences for planetary shocks and comets. J. Geophys. Res. 95, 2281–2300.

Omidi, N., Karimabadi, H., Quest, K.B., 2001. Global hybrid simulations of solar wind interaction with the magnetosphere. In: Büchner, J., Dum, C.T., Scholer, M. (Eds.), Proceedings of ISSS-6. Copernicus Gesellschaft, pp. 71–72.

Quest, K., 1985. Simulation of high-Mach-number collisionless perpendicular shocks in astrophysical plasmas. Phys. Rev. Lett. 16, 1872–1874.

Quest, K., 1988. Theory and simulation of collisionless parallel shocks. J. Geophys. Res. 93, 9649–9680.

Quest, K.B., Shapiro, V.D., 1996. Evolution of the fire-hose instability: linear theory and wave-wave coupling. J. Geophys. Res. 101, 24,457–24,469.

Rymer, A.M., et al., 2006. Correlation of electron heating and compression, bulk energy dissipation and magnetic field transition with distance down the dusk flank of the Jovian bow shock. J. Geophys. Res., in press.

Scarf, F.L., Gurnett, D.A., Kurth, W.S., Poynter, R.L., 1979. Plasma wave turbulence at Jupiter's bow shock. Nature 280, 796.

Scarf, F.L., Moses, S.L., Kennel, C.F., Greenstadt, E.W., Coroniti, F.V., 1987. Plasma waves near collisionless shocks. In: Szego, K. (Ed.), Proceedings of the International Conference on Collisionless Shocks in Balatonfured, Hungary. Central Research Inst. for Physics, Budapest, Hungary, pp. 19–41.

Shimazu, H., 2001. Three-dimensional hybrid simulation of solar wind interaction with unmagnetized planets. J. Geohpys. Res. 106, 8333–8342.

Sonnerup, B.U., Scheible, M., 1998. Minimum and maximum variance analysis. In: Paschmann, G., Daly, P.W. (Eds.), Analysis Methods for Multi-Spacecraft Data. Published for The International Space Science Institute by ESA Publications Division, Noordwijk, The Netherlands, SR-001, pp. 185–220.

Stix, T.H., 1992. Waves in Plasmas. American Institute of Physics, New York.

Szego, K., Glassmeier, K.-H., Bingham, R., Bogdanov, A., Brinca, A., Cravens, T., Dubinin, E., Fischer, C.H., Fisk, L., Gombosi, T.I., Haerendel, G., Lee, M., Mazelle, C.H., Mobius, E., Motschmann, U., Isenberg, P., Shapiro, V.D., Sauer, K., Schwadron, N., Tsurutani, B., Zank, G., 2000. Physics of mass loaded plasmas. Space Sci. Rev. 94, 429–671.

Szego, K., Young, D.T., Barraclough, B., Berthelier, J.J., Coates, A.J., McComas, D.J., Crary, F.J., Dougherty, M.K., Erdos, G., Gurnett, D.A., Kurth, W.S., Thomsen, M.F., 2003. Cassini plasma spectrometer measurements of Jovian bow shock structure. J. Geophys. Res. 108 (A7), 1287.

Young, D.T., et al., 2004. Cassini plasma spectrometer investigation. Space Sci. Rev. 114, 1–112.